Demosaicing images from colour cameras for digital image correlation

Demosaicing images from colour cameras for digital image correlation

A. Forsey*, S. Gungor

The Open University, Milton Keynes, Bucks, UK, MK7 6AA

Abstract

Digital Image Correlation is not the intended use for consumer colour cameras, but with care they can be successfully employed in such a role. The main obstacle is the sparsely sampled colour data caused by the use of a colour filter array (CFA) to separate the colour channels. It is shown that the method used to convert consumer camera raw files into a monochrome image suitable for digital image correlation (DIC) can have a significant effect on the DIC output. A number of widely available software packages and two in-house methods are evaluated in terms of their performance when used with DIC. Using an in-plane rotating disc to produce a highly constrained displacement field, it was found that the bicubic spline based in-house demosaicing method outperformed the other methods in terms of accuracy and aliasing suppression.

Keywords: Digital Image Correlation; Demosaicing; Colour Filter Array; Colour Camera.

1 Introduction

Digital Image Correlation (DIC) [1,2] is an increasingly popular technique for measuring spatially resolved surface strain. Its principle is based on computational tracking of contrasting surface features on digital images. One of the main attractions is the relatively simple equipment required and that is simply a device capable of taking suitable images, most often a camera. Typically, two or more images are acquired before and after a loading event and the relative movements of the surface features in each image are determined. High measurement accuracy relies on resolving features at a sub-pixel level. This is best achieved when the light intensity of each pixel is registered accurately, as in the case of monochrome cameras. It is possible to use colour cameras for DIC, but first the colour information must be converted into a monochrome signal and the method by which this is achieved can have a significant effect on the eventual result. Therefore, scientific monochrome cameras are predominantly used for DIC so that this processing step can be removed and because on a pixel-to-pixel comparison the colour cameras are at a disadvantage. There has been a large body of work dedicated to the measurement or estimation of error in DIC. This work generally considers the error caused by different algorithms [3], different parts of the algorithm [4,5], or methods for estimating error [6]. To the authors' knowledge there are no published studies on the effects of using colour camera for DIC other than Yoneyama [7], who use a 3 CCD colour camera rather

than one with a colour filter array (CFA). This arrangement removes the problem of sparse sampling of each colour channel, but does not represent the configuration of the majority of digital colour cameras. For cameras using CFAs, only statements in papers that have used colour cameras that allude to their effects [8] have been found.

There are situations where using a colour camera could have an advantage, but this is mainly down to grounds of cost. Due to the large market demand for colour cameras, high quality models can be obtained for a fraction of the cost of dedicated scientific cameras. These consumer cameras have a faster product life cycle and can possess a large pixel count. These cameras are not designed to take scientific measurements and so they have multiple undesirable features not found on scientific cameras. These are specifically, and not limited to, CFAs, pixel lenses, anti-aliasing filters, and a viewfinder mirror mechanism. However, for long term testing where a camera is in place for months [9,10], the cheaper colour cameras may still be an attractive proposition. With the additional resolution of these cameras, there are other situations in which they may preferable to the monochrome scientific cameras, such as crack detection. There also must be a comparable resolution at which a good quality colour camera will gain performance parity with a monochrome camera of a lower resolution, due to the higher resolution colour camera being able to use more pixels is each subregion to obtain the same spatial resolution.

2 Demosaicing

When performing DIC, a monochrome camera is preferable over a colour camera of the same resolution, unless the colour information is required for a separate purpose. These cameras are made up of photosites that all have similar sensitivity and so any speckle moving from one pixel to the next will produce a similar and predictable response. The majority of colour cameras use a CFA to make individual pixels sensitive to red, green or blue (some cameras separate to CMYK, but the principle remains the same). The arrangement of the CFA of the colour camera described in this paper is a Bayer pattern [11]. This pattern has twice the number of green photosites as red or blue arranged in a 2x2pixel repeating-unit, as seen in Figure 1. From this sparse colour sampling, a full colour image is produced by interpolating the unknown values in each colour channel. This interpolation is achieved via any one of the many demosaicing algorithms available [12–14] to calculate a red, green and blue value for every pixel position, where only data from one channel was captured. These three channels, red, green and blue, can then be combined to create a monochrome image suitable for DIC.

The requirements for the demosaicing process to perform successful DIC using a colour camera are somewhat different to that of that to create a successful photograph. A monochrome output from the camera is required and the result should be as repeatable as possible when the sample is subjected to sub-pixel shifts. The first condition is simple to achieve, the second is much more problematic due to the sparse sampling of each colour channel. One of the aims

of this study is to investigate the effect of how the colour channels are combined to produce a monochrome image for DIC and the resulting output.

For consumer cameras, the raw mosaic image can be accessed though saving images in the proprietary raw format. Many algorithms are available for producing a full colour image from these sparsely sampled colour channels caused by the CFA. For DIC, a monochrome image is required as the correlation is performed on a single regular array of data. This is so that the speckle pattern, specifically the difference in light intensity between contrasting features, moves from one pixel to the next as displacement increases. The aim of the demosaicing conversion is to allow a DIC algorithm to make the best use of the available data from the three colour channels. Two in-house methods will be tested here, bilinear interpolation and bicubic spline interpolation. These two are then benchmarked against a typical commercial package, in this case Corel Photo Paint [15]. Five other algorithms from the open source RAWtherapee software are then considered and all algorithms used are summarised in Table 1. The aim of this is not to promote or condemn the Corel software or an open source approach, merely to provide context for the other methods presented. Corel Photo Paint was chosen because of its ability to produce a suitable *tif* file that can be read by the LaVision software (16bit, monochrome, uncompressed *tif*) in a single program and as such would be a convenient choice for any user. The conversion using Corel Photo Paint was performed using software's default settings of sharpness and colour balance. RAWtherapee was chosen due to its range of demosaicing algorithms from a single open source. In this case the images were converted to monochrome *tifs* using Matlab, giving equal weight to each colour channel.

Demosaicing method	Comment	Ref
Ahd	Adaptive homogeneity directed	[16]
AMaZE	Aliasing Minimization and Zipper Elimination	[17]
Bicubic	Bicubic spline interpolation	in-house
Corel PP X4	Proprietary software	[15]
dcb	Góźdź method	[18]
eahd	Horváth's AHD	[19]
Linear	Bilinear polynomial interpolation	in-house
vng4	Variable Number of Gradients	[20]

Table 1: Summary of demosaicing algorithms considered in this investigation.

With the aim to produce a spatially consistent monochrome image, the two in-house methods considered here treat each colour channel entirely separately. The interpolation is performed in two ways, the first using bilinear interpolation and the second using bicubic splines. For both methods, each missing component of the colour channel is calculated using a different size of region for the green channel as for the red or blue. For the bicubic spline method, the extent of the regions required for interpolation of the different colour channels is illustrated schematically in Figure 2. This figure also illustrates that to calculate the sizes of the regions required to calculate the red and blue channels at a green photosite have rotational symmetry of order 2, rather than 4 as for the other two situations. The splines use only measured values in a single colour channel as

knots and are defined using the not-a-knot end condition. This process path produces a green channel that possesses twice the spatial frequency information of either the red or the blue channels. Once the RGB channels have been calculated, the channels are summed giving double weighting to the green channel due to it having twice the number of input measurement points.

As the CFA is not easily removed to provide a direct comparison of the performance of a true monochrome camera, a second camera will be used to perform this role. By comparing these two cameras perhaps a more important comparison can be made between the two potential options faced by DIC users when selecting cameras for their needs.

3 Experimental

To enable a direct comparison between different demosaicing algorithms and cameras, a test is required with a well-characterised solution. For this reason a plate with a painted speckle pattern applied to the surface was rotated about the normal of the lens in the object plane. Once the displacement vectors were produced using DIC, a first-order two-dimensional polynomial was fitted to the data using the least-squares method. No deformation was applied to the plate and it was rotated in plane and so, due to the large number of nearly independent data points across the image, the fitted plane can be taken as a very close approximation to the true displacement of the plate. The calculated displacement vectors can then be subtracted from the "true" displacement of the plate with the result henceforth referred to as least-squares error (LSE).

3.1 Cameras

Both the cameras tested use the same lens-mount and have a similar sized sensor so a direct comparison is possible with the same optical setup. This results in a very similar region of interest available for each for each camera. The pixel count and therefore pixels size will differ, but the cameras are the highest resolution colour and monochrome cameras currently available with this mounting system. For this reason, comparing a 16-megapixel monochrome image to a 36-megapixel colour image is reasonable as the aim is to compare the maximum achievable DIC resolution. The drawback of this method for comparison is that the two cameras will produce images with different speckle sizes in terms of pixels. To mitigate this the in-house demosaicing algorithms were also used on the monochrome images by treating the image as if it had been taken with a CFA on the sensor.

The cameras used in this investigation were all manufactured by Nikon, this was because they use the same "F-mount" and so could be interchanged without changing the focus or working distance of the lens. A similar effect may be seen using cameras made by different manufacturers, but that has not been addressed here.

The Nikon DSQi2 is a 16-megapixel monochrome microscope camera based on Nikon's consumer camera technology and CMOS sensors. However, it differs from the DSLR (Digital Single Lens Reflex) cameras in that the sensor also

resides in a number of ways that make it more suitable for DIC. Primarily the CFA is removed so it is a true monochrome camera; similarly the anti aliasing filter and pixel micro-lenses have also been removed. The body is designed for use on a microscope and so no mirror or physical shutter are present to induce vibration into the system. The sensor is also electronically cooled to prevent a built up of heat due to prolonged use from increasing the readout noise in the image.

The Nikon D810 digital single lens reflex (DSLR) camera is a 36 megapixel colour consumer camera. It has a CFA using a Bayer pattern with individual microlenses on each photosite to increase the amount of light gathered for each pixel. These microlenses help increase the effective fill factor of the sensor at the expense of uniformity of response across the light sensitive region of the photosite.

The same optical path setup was used for all tests. This was comprised of a Nikon 200mm micro f4 lens. Illumination was provided using a 150W light box with a 0.5" diameter fibre optic light guide so no heat or thermal currents were introduced into the imaging system and a working distance of 600mm. The speckle pattern was produced on a 1mm thick aluminium sheet using matt anti-rust aerosol paint. First a white base was applied across the surface, followed by a black speckle. Many passes of the black paint were used to slowly build up a dense speckle pattern. The paint was not sprayed directly toward the sample surface, instead it was aimed below so that only the small light paint particles in the overspray form part of the speckle pattern. In this way the speckle pattern can be kept more consistent.

3.2 Procedure

The experimental procedure involved incrementally rotating the speckle pattern using a rotation stage and taking images at each rotation step. In order to prevent bias in the error analysis to be introduced by small differences in rotation it was decided to remove and replace the cameras at each rotation step. With the lens firmly mounted to the same rail as the rotation stage the cameras (see Figure 3) could be replaced more accurately than the rotation could be reproduced. The cameras were removed and replaced before each image was taken so each image underwent the same disturbance.

Sixteen images for each camera were recorded and passed through the various demosaicing filters to produce 11 sets of images. Each set of images was processed using DaVis 8.2 [21] least squares method [2,22,23] using parameters outlined in Table 2, for subregion sizes of 11, 15, 21, 31, 41, 51 and 61, all at a 7 pixel stepsize. These data were then exported to Matlab [24] where a plane was fitted to the data.

Algorithm parameter	Value
Pyramid levels	1
Epsilon	0.01
Correlation threshold	0.2
Subregion shape	Round
Subpixel interpolation	Bicubic spline

Subregion scale normalisation	On
Step size	7

Table 2: Summary of common DIC algorithm parameters for all analyses.

To provide context to the comparison between the monochrome camera and the demosaiced colour images, two of the demosaicing algorithms have been applied to the monochrome images. The monochrome image was split into three channels, each one an analogue of a colour channel from a colour camera and taken from the same position on the image sensor. This produced two channels with similar numbers of data points to represent the red and blue channels and a third channel with twice as many data points to represent the green. These mosaiced images were then processed using the linear and bicubic demosaicing algorithms used on the true colour cameras. In this way the demosaicing algorithms can be directly compared with monochrome data from the same image.

4 Results

The global measured displacement as calculated for each camera and demosaicing algorithm using the polynomial fit, can be seen in Figure 4a. The increase in rotation is not linear and appears to have two rotation steps that are significantly smaller than the rest, specifically frames 2 to 3 and 10 to 11. Overall values of rotation are extremely consistent for each camera across differing demosaicing algorithms. There is a small discrepancy between the results of rotation from the monochrome camera and the colour camera. Figure 4b shows the absolute difference in the measure of rotation between the different approaches is at a maximum for smaller values of rotation and decreases as more rotation is applied. The values in this plot are all relative to the average for the appropriate image (the value from Figure 4a) and so should be taken as comparative as the “true” value is not known.

Measurement of the in plane rotation of a flat plate produces a highly constrained vector field. This was done to simplify the error analysis, but it also has the benefit that the error, and the progression of the error, can be visualised by considering the asymmetric parts of the strain tensor. Figure 5 shows the procession of error (Least Square Error – LSE) across the surface for different applied rotation for the 61x61 pixel subregion analysis of the y-direction displacements of the colour camera images. Aliasing can be seen in the form of the repeating peak-valley “dotted” pattern. For each algorithm, this pattern remains similar in magnitude but increases frequency as rotation is applied. It is also apparent that the demosaicing method has a large effect on the amplitude of aliasing observed, with the two in-house algorithms clearly producing less prominent aliasing effects than the other methods considered. From the sample speckle shown for each analysis it can be seen that the monochrome camera produces a higher contrast image than the processed colour cameras.

Figure 6 shows the common aliasing, or peak-locking, effect [25] as seen to greater or lesser extent for all cameras used for DIC, caused primarily by interpolation error [5]. This plot shows the histogram of the normalised percent

of vectors from all 15 images that are present in the data at twenty incremental sub-pixel displacement values. This shows the difference in the measured to the expected number of vectors present in each bin. Part *a* of the plot shows varying degrees of integer pixel bias for the 11x11 pixel subregions for the different cameras and demosaicing algorithms. The generic algorithms suffer from a greater amount of aliasing than the in-house linear and bicubic algorithms. The raw monochrome camera has the highest overall degree of aliasing and this is reduced by the application of the in-house demosaicing algorithms. Part *b* of this figure shows that this effect no longer present using the 61x61 pixel subregions.

Figure 7 shows similar data to Figure 6, but instead of binning over a single pixel all the data is binned in 20 increments across 2 pixels. This is done because of the 2x2 repeating minimum unit of the CFA on the colour camera. It is clear from both parts *a* and *b* of the figure that the colour camera suffers considerably more aliasing at this scale than the monochromatic comparison. The generic demosaicing algorithms show greater bi-integer bias than the linear or bicubic in-house algorithms, with the dcb method showing the greatest control of this effect. The monochrome camera, as would be expected due to its lack of CFA, shows no bi-integer bias effect. In this figure it reveals its integer bias as an effect at twice the frequency of the colour cameras. The effect is not present even when the monochrome raw data is put through the same demosaicing algorithms as the colour camera data. Bi-integer bias is reduced for the 61x61 pixel subregions in part *b* of the figure in comparison to that in part a at 11x11 pixels.

Figure 8*a* the variation of the zero displacement values with the subregion size. These were computed from the histograms at each subregion size, of which 11x11 and 61x61 are from Figure 6*a* and 4*b*, respectively. This shows the relative degree of aliasing present for different cameras and algorithms at the various subregion sizes. The integer bias rapidly drops to zero for the demosaiced monochrome images, while the raw monochrome images continue to reduce throughout the subregion size range. The generic algorithms show higher levels of integer bias, which does not change considerably with subregion size. The linear algorithm shows the opposite trend to other methods in that the peak value increases with increasing subregion size. The bicubic approach shows a stable value of aliasing that is both lower than any of the other colour camera data and also more consistent.

Figure 8*b*, similar to Figure 8*a*, shows the zero displacement values for the bi-integer bias histograms of Figure 7*a*, Figure 7*b*, and those subregion sizes between. The monochrome camera, both raw and demosaiced show the lowest levels of bi-integer bias. Bicubic spline, linear and the dcb approaches show similar and consistent levels of aliasing that are virtually insensitive to subregion size. The remaining algorithms show a significantly larger effect that reduces with increasing subregion size.

Figure 9*a* shows the average least squares error (LSE), the absolute mean difference between the plane fit and the displacement vectors, for varying subregion sizes and for all algorithms. All methods show a gradual decrease in LSE with increasing subregion size. For subregion sizes below 31x31 pixels,

bicubic and bilinear colour camera demosaicing show lower LSE than the monochrome camera. At subregion sizes greater than this the monochrome camera produces a lower value. Figure 9*b* shows the same data as Figure 9*a*, but converted into true object plane scaling in mm. The smaller pixel size of the colour camera reduces all the LSE values of the colour camera to well below that of the monochrome camera. In this plot the lowest value of LSE is found from the colour camera using bicubic spline demosaicing for all subregion sizes.

5 Discussion

The rotation measured for each image, as shown in Figure 4a, shows a discrepancy between the monochrome and colour cameras. This is due to the experimental method where each camera was removed and replaced before each image was taken. To do this, the cameras are rotated in relation to the lens to a hard stop on the mount, so any inconsistency in the amount of rotation between the two cameras will largely be due to float in the clip mechanism at this hard stop. The measurement of rotation appears not to be affected by the choice of demosaicing algorithm and this is not surprising due to the number of vectors involved in this calculation. This validates the assumption that a fit used in this way can be used as the "true" displacement for the subsequent analyses. The two steps that experience a smaller rotation step than the others, specifically 2 to 3 and 10 to 11, are seen equally by both cameras and so this is an artefact of slack in the take-up in the gears of the rotation stage used for the experiment. A beam splitter could have been used to eliminate this problem caused by float in the mechanism, but then the optical path would differ between cameras and any chromatic aberration caused by the beam splitter would disproportionately affect the colour camera.

Figure 4b shows that the effect on rotation measurement of the different demosaicing approaches is at its highest for small rotations. The greater spread of sub-pixel displacement values and the low signal to noise ratio caused by measuring such small displacements emphasising systematic biases is likely the dominant cause of this phenomena. However, the only difference between the analyses for each camera is the demsaicing process, as the same images are used, so this must be the ultimate root of the effect.

It is outside the scope of this experiment to produce universal error values for different cameras or algorithms. The data presented here are for comparative purposes only and only hold true for this speckle pattern and the processing methods used. However, it can be used to rate the relative performance of each algorithm. This is not a true test of camera performance due to the difference in effective speckle size because of the differing pixel sizes between the cameras, but this does not prevent some conclusions being made.

In Figure 6, the demosaiced monochrome image suffers less of an integer bias effect than the raw data. This is most likely due to the smoothing effect of the demosaicing methods and not some intrinsic property of the demosaicing process. A similar effect would most likely have been observed if the lens was de-focussed by a small amount to blur the sharp contrasts of the painted speckle

pattern. That the monochrome camera shows a larger effect than any of the colour algorithms owes more to the difference in effective speckle size between the two cameras. To perform this test, a balance had to be struck when prescribing the speckle size on the sample surface that will enable both cameras to perform well despite their difference in resolution: this is a result of that compromise.

The linear and bicubic demosaicing methods show the least integer pixel bias for this set of images, but as can be seen in Figure 8*a*, the linear method is not consistent for all subregion sizes. It is not clear why this would be the case as the demosaicing method itself is very similar to the bicubic spline algorithm, which does not display this effect.

Bi-integer bias is present in differing amounts for all demosaicing algorithms for the colour camera as seen in Figure 7. In Figure 8*b* it can be seen that the magnitude of the bias reduces with increasing subregion size for the generic demosaic algorithms, but is constant for both the linear and bicubic approaches. This is because the former have been developed for increasing sharpness and supressing colour fringing, as opposed to spatial consistency.

Bi-integer bias is not present for the monochrome camera in Figure 7 and the periodicity that is visible is due to the single integer bias as discussed previously that is manifest as a feature with twice the frequency of the bi-integer bias from the colour camera. Bi-integer bias is not even produced from the monochrome image when it is split into three simulated colour channels to approximate the colour camera and processed using the two in-house demosaicing algorithms. This shows that this bi-integer bias is not a product of the sparse sampling and recombination process that takes place in the colour camera, rather it is caused by some other aspect of the colour camera that has not been simulated here. The likely responsible feature is the CFA itself and the difference in contrast that occurs when part of a speckle moves from one coloured pixel to a different coloured pixel. Even with a true black and white speckle pattern, the difference in response of the photosites to different colours would produce different intensities from the same input. For the colour camera there is also the complication of microlenses on each photosite to increase its sensitivity, but these are unlikely to produce the bi-integer bias, as the effect would be similar for each colour channel. This would suggest that an algorithm that would work in a similar manner to the bicubic method considered here, but that could correct for the difference in contrast as seen by the filters of in the CFA might reduce this effect still further and produce an even better tool for use with DIC.

The bicubic spline based algorithm shows a reduction in integer and bi-integer aliasing in comparison to the other methods tested here. The effect of which can be seen arbitrarily in Figure 5. This illustrates the 2D nature of the bi-integer bias effect and how it may manifest in regions of constant strain, such as this idealised situation of the rotating disk.

The higher contrast images from the monochrome camera are a result of the broader frequency sensitivity of the monochrome sensor. When using a colour

sensor the illumination is always a compromise because the photosites are not uniformly sensitive to all frequencies of light, in particular they are least sensitive to the blue end of the spectrum. The photosites that provide the information to make up this channel are only sensitive to the blue spectrum and so this part of the image produces poorer contrast than the green. A similar, but less significant effect also occurs with the red channel. If the illumination were tuned to allow equal illumination for each colour channel, the contrast in the colour camera images could be improved and so lead to an improvement in DIC performance as a result.

In Figure 9*a* it appears that the bicubic and bilinear demosaiced colour cameras outperform the monochrome camera on a pixel to pixel basis. This is most likely due to the difference in speckle size between the two cameras, in particular the speckle in the monochrome image being small, in combination with sharp delineations between light and dark areas. This comparison is also not as direct as between the differently demosaiced colour images because it is calculated from a different image taken by a different camera and so no such strong conclusions can be made. What can be said is that the LSE of the monochrome camera in this test is comparable to the colour camera using the very best demosaicing algorithm. Considering that the monochrome camera images possess a compromised speckle pattern to enable the comparison, it is most likely that the pixel-to-pixel performance in comparison to the colour camera would be slightly superior in more directly comparable conditions.

LSE is predominantly determined by the degree of aliasing present in the results, a convolution of both integer bias and bi-integer bias, and as such a similar trend can be seen in the performance of the demosaicing algorithms by this measure. The difference with the LSE measure is that it permits comparison of the combined result of all these effects with an output in terms of displacement. The difference between the raw monochrome camera results and the demosaiced data from these images shows what an effect having a speckle pattern with smooth transitions from peak to peak can improve DIC results.

LSE is measured in pixels and so this can be scaled into object plane coordinates in millimetres, the result can be seen in Figure 9*b*. This shows that while the aliasing is large for some of the algorithms, it is not large enough to entirely offset the increased resolution boasted by the colour camera. To get the same spatial resolution with the same sized region of interest, the monochrome camera shows considerably more LSE at all subregion sizes. As LSE is primarily linked to aliasing, it shows that while the aliasing of some of these demosaicing algorithms is significant, when scaled to the object plane it is still less than the lower resolution monochrome camera. This is partially because the same fraction of a pixel aliasing has a smaller effect in the colour camera, because the pixel is smaller. Also when comparing the cameras at the same spatial resolution, the colour camera uses more pixels and so a larger subregion for the same calculation. These effects combined together show produce a large net difference in the DIC performance of the two cameras.

To recreate the speckles from the sample surface with as little positional or intensity bias as possible is the aim of a demosaicing algorithm when using colour cameras for DIC. As can be seen from the results presented here, this is not easy to achieve. The in-house developed bilinear and bicubic algorithms outperform the proprietary and open source algorithms considered here in both bias and displacement error. These in-house algorithms use interpolation schemes that are utilised for subpixel interpolation within commercial DIC algorithms and so were likely to be suitable candidates for this processing step also. The bicubic method has been shown to be superior in terms of single pixel aliasing and so this method would be recommended for this camera system and speckle pattern. As the demosaicing process described here is performed offline, increasing the order of the interpolation to biquintic splines may further improve the results.

It can be seen from the decreased integer bias seen in Figure 6*a* and lower LSE in Figure 9 for the monochrome camera data due to the demosaicing algorithms, that the nature of the speckle pattern can have a significant effect on the DIC data. In this case it is due to the smoothing effect of the demosaicing algorithms on the raw image and so producing more gradual changes in intensity, which are better characterised by the interpolator used in the DIC algorithm [5]

The difference in pixel size, and so resolution, between the two cameras makes direct comparison more complicated than direct pixel-to-pixel mapping. However, this is a relevant question because these two cameras represent a high-resolution option from their respective genres. The two cameras have a very similar sized sensor and share the same mount, so these variables have been kept consistent even if the resolution has not. This combined with the four-fold price difference between the two cameras (at time of writing) in the colour camera's favour show that these two cameras could be considered competitors for the attention of a DIC practitioner. Consumer colour cameras such as the Nikon D810 as considered here are not specifically designed for DIC and so they have features that would make them unsuitable for many DIC applications. Large file sizes and moving parts reduce the maximum usable frame-rate to the region of 1Hz, which lends them to quasi-static or long term testing. For long term testing consumer cameras become more attractive due to the lower investment required for a single test. However, colour cameras can only be taken seriously for DIC if their performance and accuracy features are well understood. The bicubic spline demosaicing algorithm considered here is a step towards this goal.

6 Conclusion

Colour cameras can be successfully used for DIC, but the demosaicing method used to produce the monochrome input image can have a significant effect on the DIC results. Bi-integer bias is the largest cause of error for these colour images and this is a process not seen with monochrome cameras. The single integer bias seen in the colour camera is of the same order of magnitude as that seen in monochrome cameras, and in this case specifically it was less. This is particularly relevant as a histogram across a single pixel is generally used to determine the presence of integer bias for DIC. If this were performed for colour cameras it

would appear that there was very little bias, when if the histogram is extended to two pixels then a very strong bias can be observed. To reduce these effects as far as possible, a bicubic spline based interpolation demosaicing algorithm has been proposed. This algorithm has been shown to outperform all other considered methods in terms of aliasing and accuracy. More trials involving cameras with varying sensor sizes and resolutions are required before this could be confidently recommended more widely, but the results shown here are promising in that regard.

7 References

[1] Peters WH, Ranson WF. Digital imaging techniques in experimental stress analysis. Opt Eng 1982;21:427–31.

[2] Sutton MA, Schreier H, Orteu JJ. Image Correlation for Shape, Motion and Deformation Measurements: Basic Concepts,Theory and Applications. Springer; 2009.

[3] Hild F, Roux S. Digital Image Correlation: from Displacement Measurement to Identification of Elastic Properties – a Review. Strain 2006;42:69–80.

[4] Schreier H. W. SMAWYQBHA. Quantitative Error Assessment in Pattern Matching: Effects of Intensity Pattern Noise, Interpolation, Strain and Image Contrast on Motion Measurements. Strain 2009;45:160–78.

[5] Schreier HW, Braasch JR, Sutton MA. Systematic errors in digital image correlation caused by intensity interpolation. Opt Eng 2000;39:2915–21.

[6] Wieneke B, Prevost R. DIC Uncertainty Estimation from Statistical Analysis of Correlation Values. Adv. Opt. Methods Exp. Mech. Conf. Proc. Soc. Exp. Mech. Ser., vol. 3, 2014, p. 125–36. doi:10.1007/978-3-319-00768-7.

[7] Yoneyama S, Morimoto Y. Accurate Displacement Measurement by Correlation of Colored Random Patters. JSME Int J 2003;46:178–84. doi:10.1299/jsmea.46.178.

[8] White DJ, Take WA, Bolton MD. Soil deformation measurement using particle image velocimetry (PIV) and photogrammetry. Géotechnique 2003;53:619–31.

[9] Sakanashi Y, Gungor S, Bouchard PJ. Measurement of Creep Deformation in Stainless Steel Welded Joints. Proc. SEM Annu. Conf. June 13-16, 2011 Mohegan Sun, Uncasville, Connect. USA, vol. 5, 2011, p. 415–22. doi:10.1007/978-1-4614-0228-2.

[10] Bouchard PJ, Sakanashi Y, Gungor S. Spatially resolved creep deformation of a thick section stainless steel welded joint. 3rd Int. ECCC - Creep Fract. Conf. Rome, 2014.

[11] Bayer B. Colour imaging array. 3971065, 1975.

[12] Gunturk BK, Glotzbach J, Altunbasak Y, Schafer RW, Mersereau RM. Demosaicking: Color filter array interpolation. IEEE Signal Process Mag 2005;22:44–54. doi:10.1109/MSP.2005.1407714.

[13] Dubois E. Frequency-domain methods for demosaicking of bayer-sampled color images. IEEE Signal Process Lett 2005;12:847–50. doi:10.1109/LSP.2005.859503.

[14] Kimmel R. Demosaicing: Image reconstruction from color CCD samples. IEEE Trans Image Process 1999;8:1221–8. doi:10.1109/83.784434.

[15] Corel Corporation. Corel Photo Paint X6 2012.

[16] Hirakawa K, Parks T. Adaptive homogeneity directed demosaicing algorithm. Image Process IEEE Trans 2003;3.

[17] Martinec E, Lee P. AMAZE demosaicing algorithm 2010.

[18] Góźdź J, Rodriguez LS. Dcb demosaicing algorithm 2010.

[19] Horváth G. eahd demosaicing algorithm 2010.

[20] Chang E, Cheung S, Pan D. Color filter array recovery using a threshold-based variable number of gradients. Proc. SPIE, 1999.

[21] LaVision. StrainMaster 8.2. Goettingen: LaVision GmbH; 2014.

[22] Fleet DJ, Weiss Y. Optical Flow Estimation. Handb. Math. Model. Comput. Vision., Springer; 2005, p. 239–58.

[23] Bouguet J-Y. Pyramidal Implementation of the Lucas Kanade Feature Tracker Description of the algorithm. 2000. doi:10.1016/j.tim.2005.08.009.

[24] Mathworks Inc. MATLAB 2013a 2013.

[25] Fincham AM, Spedding GR. Low cost, high resolution DPIV for measurement of turbulent fluid flow. Exp Fluids 1997;23:449–62.

8 Figures

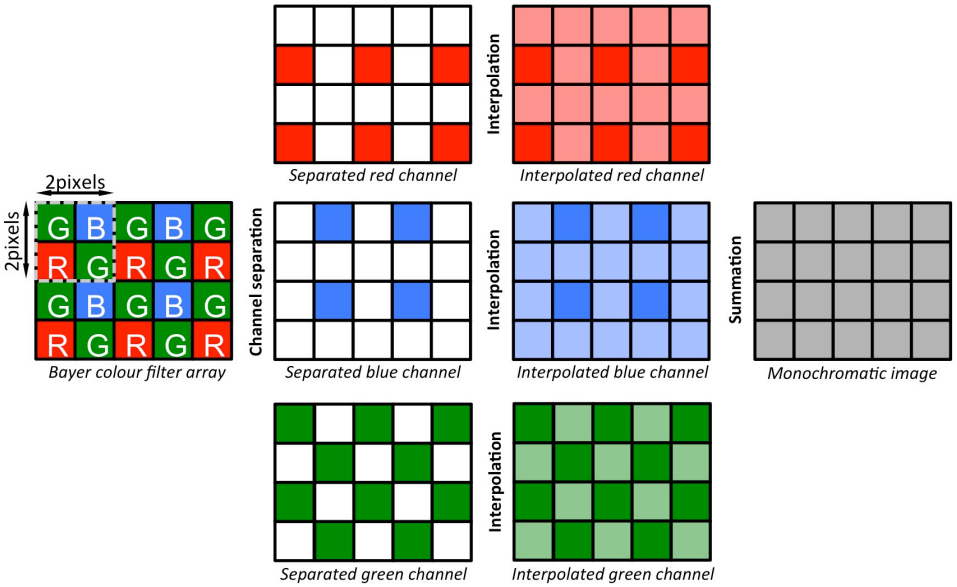

Figure 1: Schematic of Bayer colour filter array (with the 2x2 pixel repeating unit highlighted with dashed outline) showing how it is used in the in-house bilinear and bicubic spline demosaicing methods.

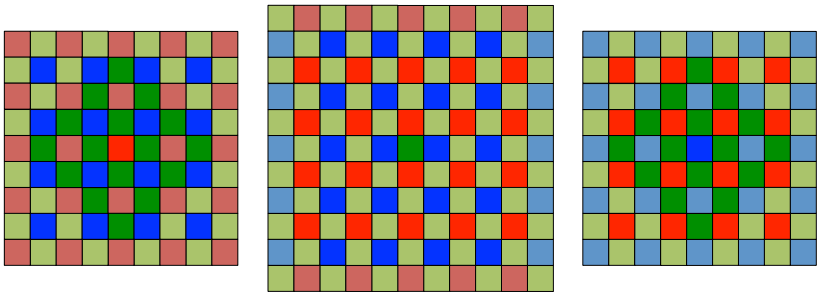

Figure 2: Schematic diagram of the pixels knots the bicubic spline demosaicing method uses to interpolate the two unknown colour channels for the three possible configurations: *left* for a pixel where the red channel value is known, *centre* for a pixel where the green value is known and *right* for a pixel where the blue value is known. Note the difference in sampled area when interpolating the green channel in comparison to the green and red channels.

Figure 3: Image of experimental setup, visible is the Nikon D810 colour camera, macro bellows, Nikon 200mm f4 macro lens, light box, fibre optic light guide and rotation stage with target.

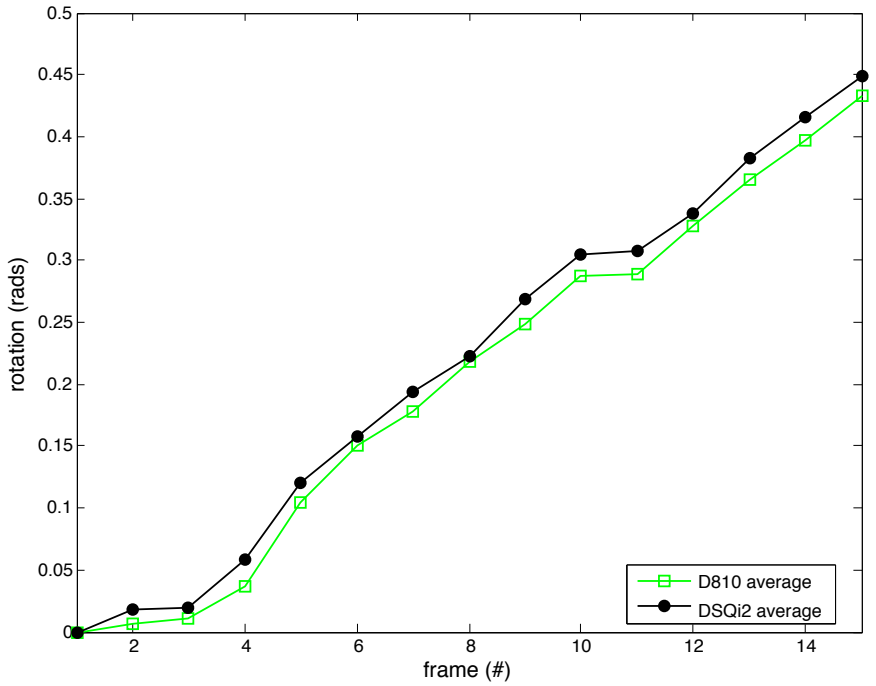

a

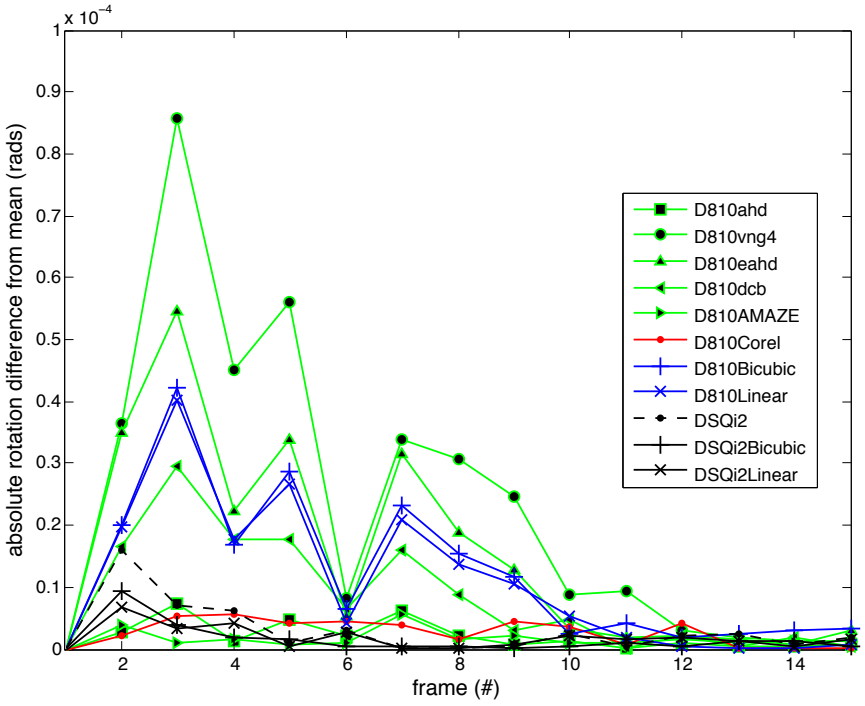

b

Figure 4: a) Global rotation measured for each camera by averaging the results of all analyses for the respective camera b) Absolute difference in global rotation measured using the different demosaicing algorithms to the mean for the corresponding camera.

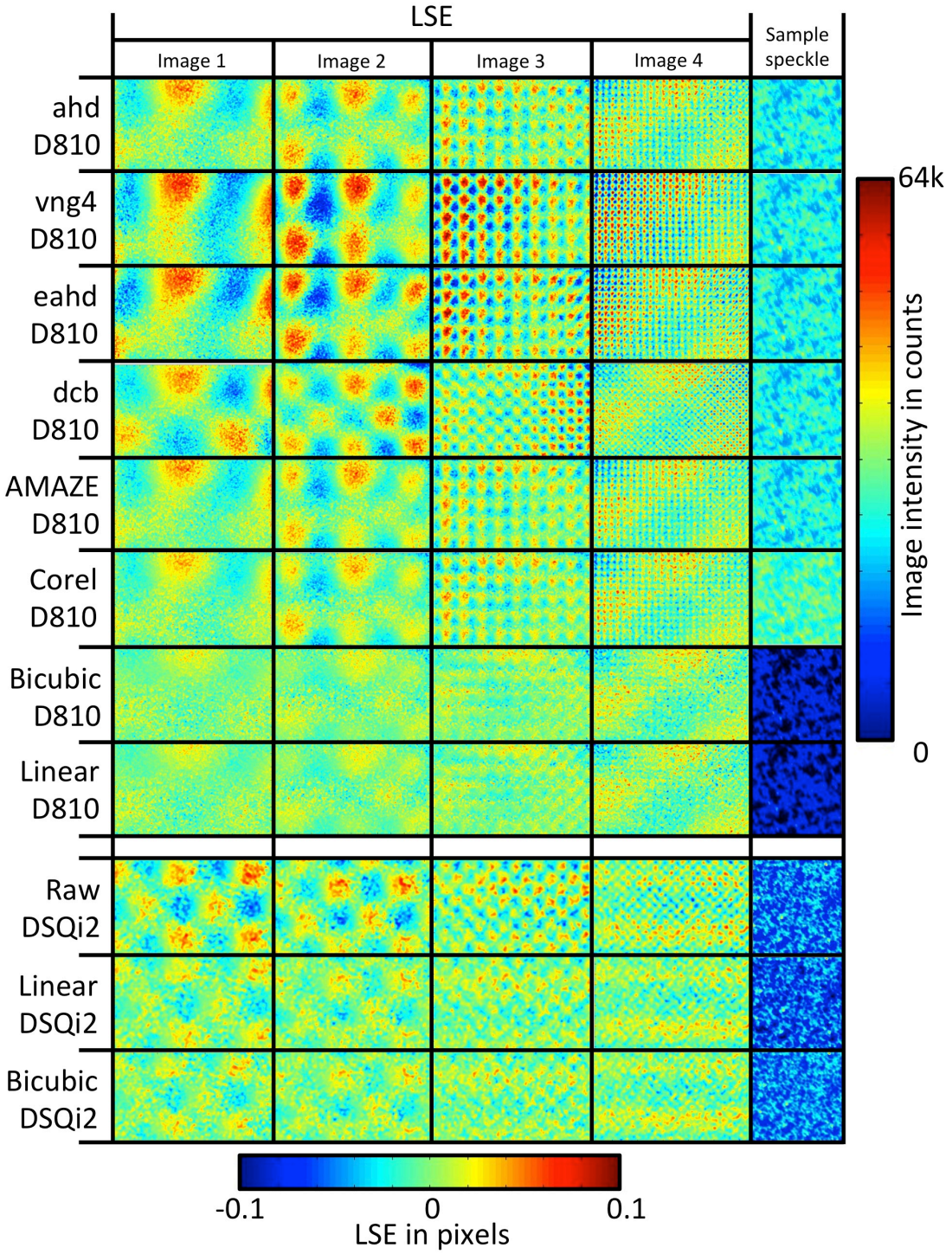

Figure 5: 2D plots of LSE in the y direction of 61x61 subregion size analysis using a 7 pixel step size for all the analyses for the first 4 rotation steps (entire images). Also included is a 150x150 pixel section of speckle pattern for each demosaicing algorithm for comparison.

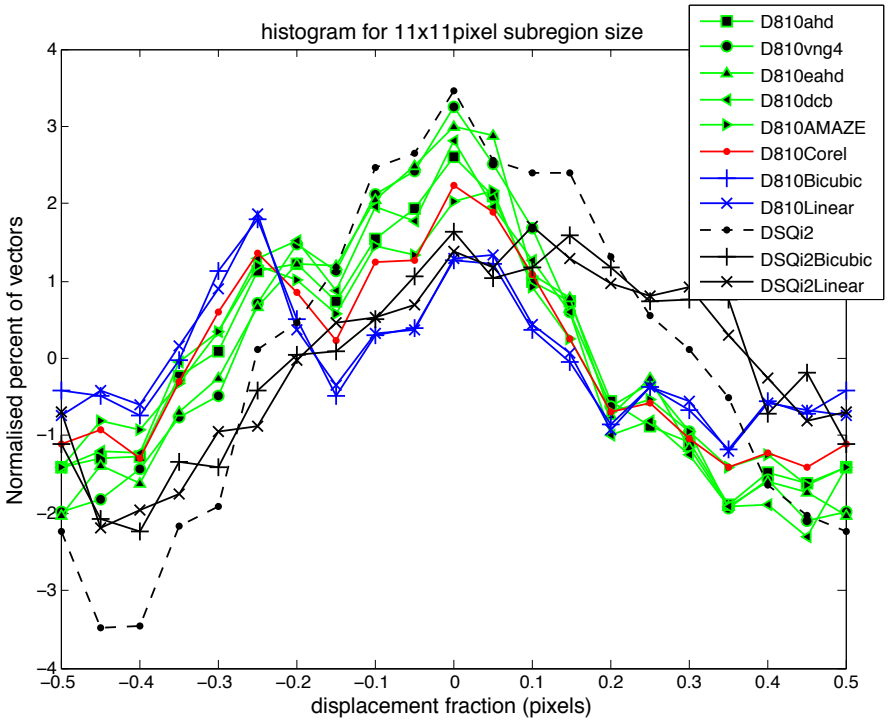

a

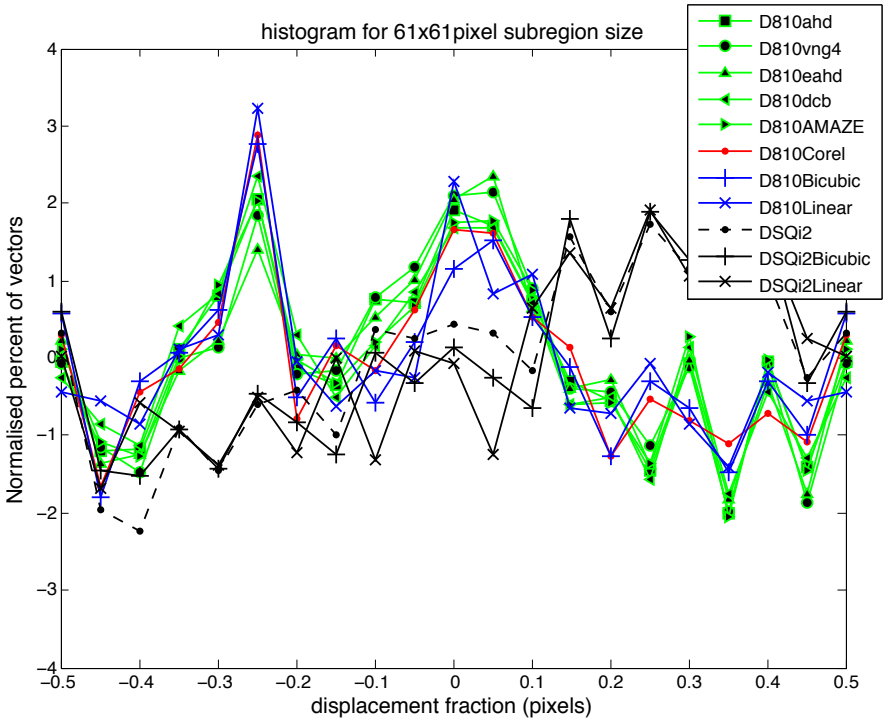

b

Figure 6: Histogram of the normalised per cent of vectors binned from -0.5 to +0.5 pixel displacement for a)11x11 and b)61x61 pixel subregions, showing the percentage of vectors in each bin in comparison to the ideal fit.

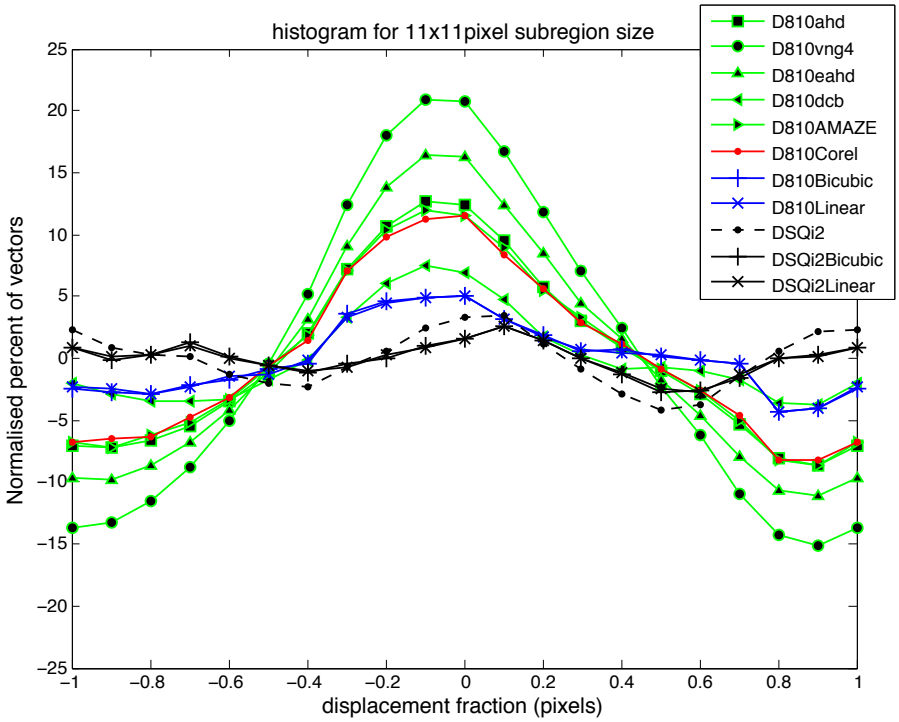

a

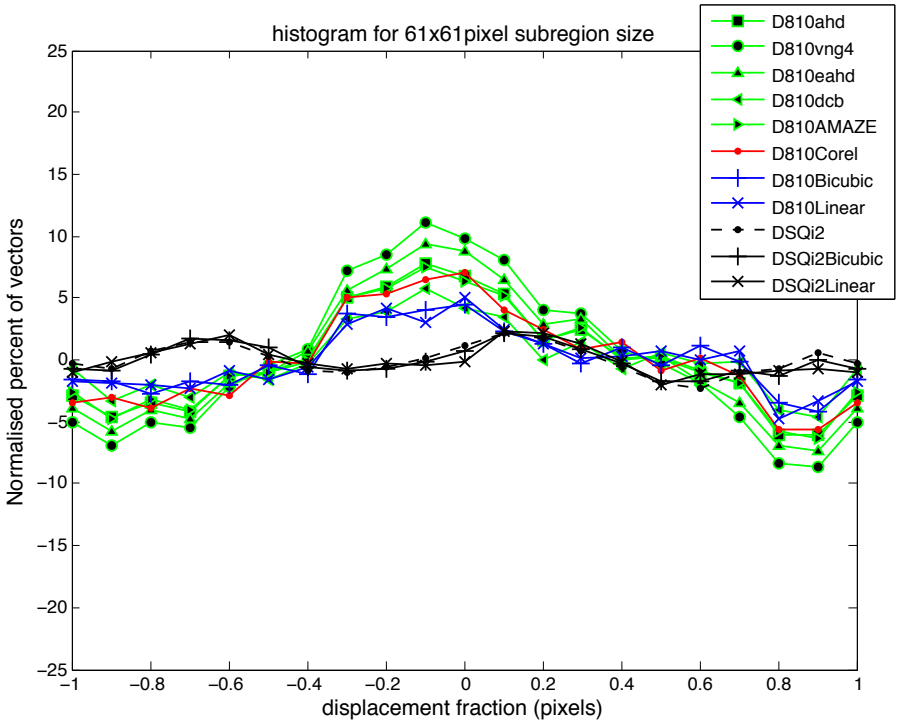

b

Figure 7: Histogram of the normalised per cent of vectors binned from -1 to +1 pixel displacement for a)11x11 and b)61x61 pixel subregions, showing the percentage of vectors in each bin in comparison to the ideal fit.

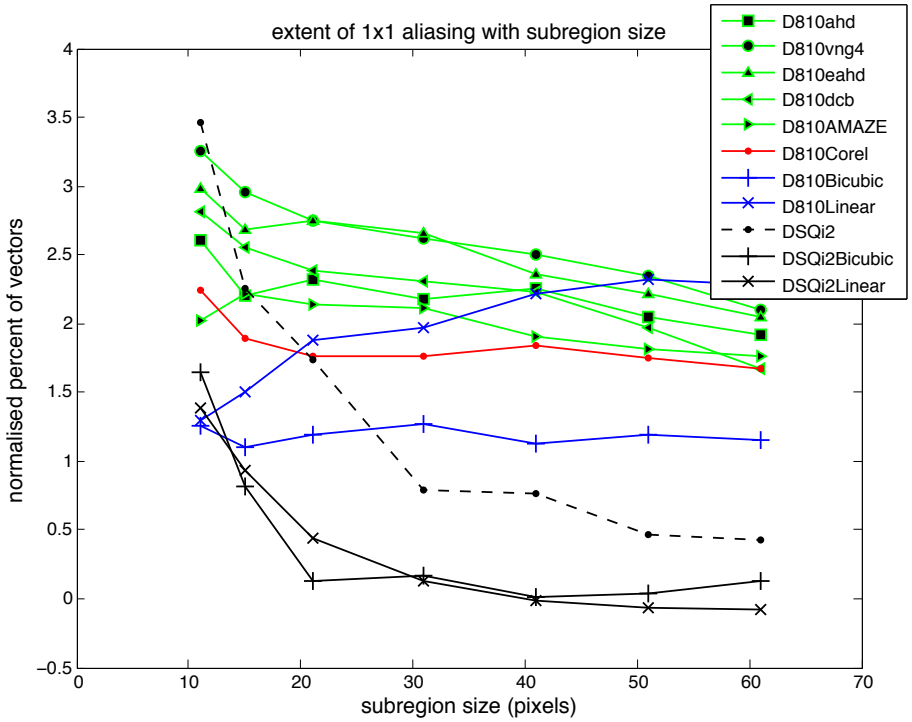

a

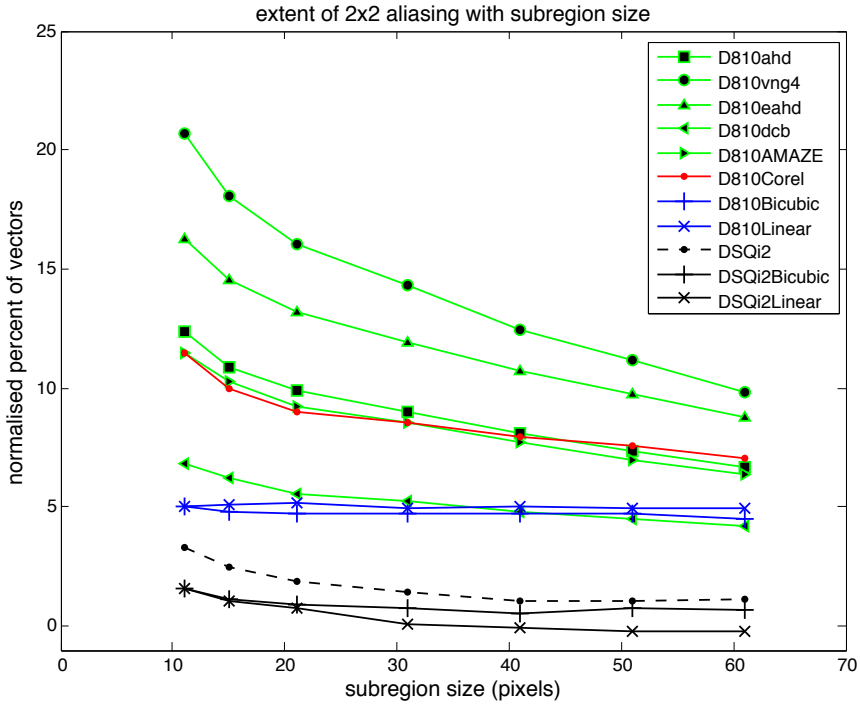

b

Figure 8: Values from the zero displacement fraction bins of the histograms in a) Figure 7 (binned from -0.5 to 0.5 pixel displacement) and b) Figure 8 (binned from -1 to +1 pixel displacement).

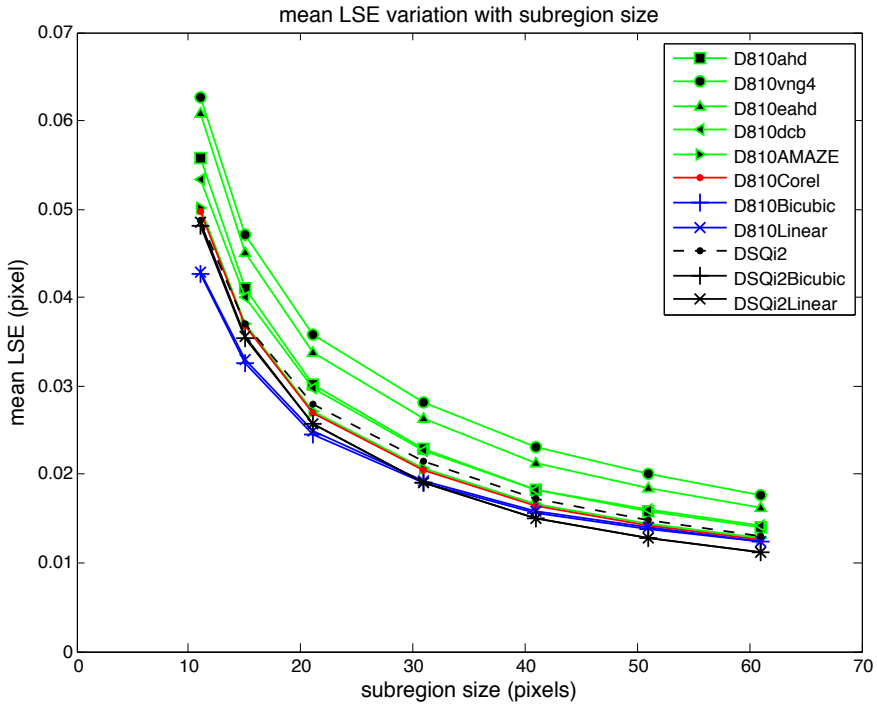

a

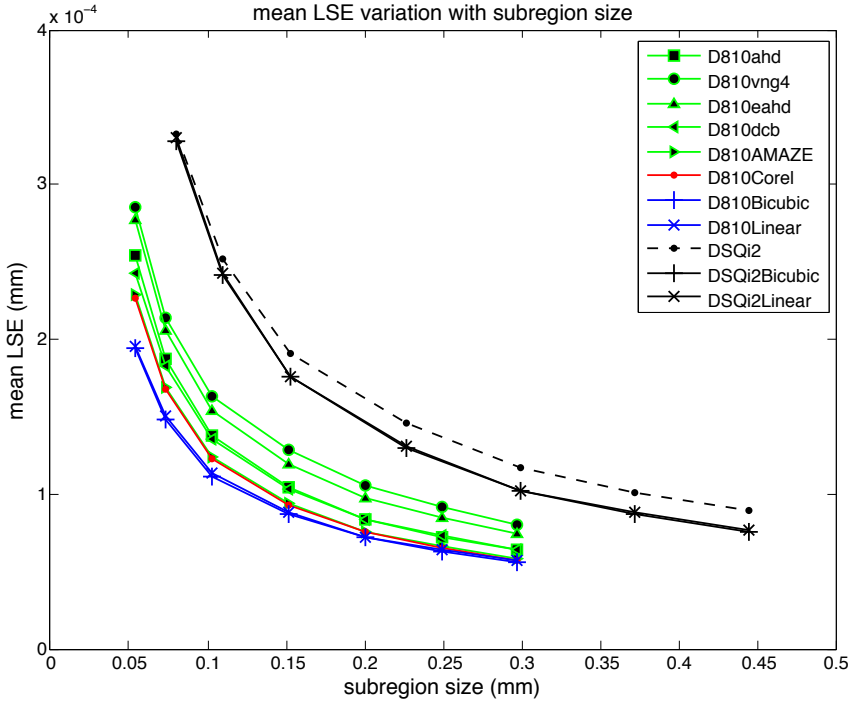

b

Figure 9: Average across entire area of all 15 images mean least squares error for all cameras and demosaicing algorithms considered for different subset sizes a) in pixels and b) in mm.